



Rain-on-snow response to a warmer Pyrenees

Josep Bonsoms¹, Juan I. López-Moreno², Esteban Alonso-González³, César Deschamps-Berger², Marc Oliva¹

¹ Department of Geography, Universitat de Barcelona, Barcelona, Spain

² Instituto Pirenaico de Ecología (IPE-CSIC), Campus de Aula Dei, Zaragoza, Spain

³ Centre d'Etudes Spatiales de la Biosphère (CESBIO), Université de Toulouse, CNES/CNRS/IRD/UPS, Toulouse, France.

Corresponding author: Juan I. López-Moreno (nlopez@ipe.csic.es)

1 **Abstract.** Climate warming is changing the magnitude, timing, and spatial patterns of mountain snowpacks.
2 A warmer atmosphere may also lead to precipitation phase shifts, with decreased snowfall fraction (Sf). The
3 combination of Sf and snowpack decreases directly affects the frequency and intensity of rain-on-snow (ROS)
4 events, a common cause of flash-flood events in snow dominated regions. In this work we examine the ROS
5 patterns and sensitivity to temperature and precipitation change (delta-change) in the Pyrenees using a
6 physical-based snow model forced with reanalysis climate data perturbed following 21st century climate
7 projections for this mountain range. ROS patterns are characterized by their frequency, rainfall quantity and
8 snow ablation. The highest ROS fr for the baseline climate period (1980 – 2019) are found in South-West high-
9 elevations sectors of the Pyrenees (17 days/year). Maximum ROS rain is detected in South-East mid-elevations
10 areas (45 mm/day, autumn), whereas the highest ROS ablation is found in North-West high-elevations zones
11 (- 10 cm/day, summer). When air temperature is increased from 1°C to 4°C, ROS rain and frequency increase
12 at a constant rate during winter and early spring for all elevation zones. For the rest of the seasons, non-linear
13 responses of the ROS frequency and ablation to warming are found. Overall, ROS frequency decreases in the
14 shoulders of the season across eastern low-elevated zones due to snow cover depletion. However, ROS
15 increases in cold, high-elevated zones where long-lasting snow cover exists until late spring. Similarly,
16 warming triggers fast ROS ablation (+ 10% per °C) during the coldest months of the season, high-elevations,
17 and northern sectors where the deepest snow depths are found. On the contrary, slow, and non-changes in ROS
18 ablation are expected for warm and marginal snowpacks. These results highlight the different ROS responses
19 to warming across the mountain range, suggest similar ROS sensitivities in near mid-latitude zones, and will
20 help anticipate future ROS impacts in hydrological, environmental, and socioeconomic mountain systems.

21

22 **Keywords:** Snow, Rain-on-snow, Climate warming, Snow sensitivity, Mountain snowpack, Pyrenees.

23

24 1 Introduction

25

26 Mountain snowpacks supply large hydrological resources to the lowlands (García-Ruiz et al., 2015; Viviroli et
27 al., 2011), with important implications in the ecological (Wipf and Rixen, 2010), hydrological (Barnett, 2005;



28 Immerzeel et al., 2020) and socioeconomic systems by providing hydroelectricity (Beniston et al., 2018) or
29 guaranteeing winter tourism activities (Spandre et al., 2019). Climate warming, however, is modifying
30 mountain snowfall patterns (IPCC, 2022), through temperature-induced precipitation changes from snowfall
31 to rainfall (Lynn et al., 2020), leading in some cases to rain-on-snow (ROS) events. The upward high-latitude
32 temperature and precipitation trends (Bintanja and Andry, 2017) and mountain elevation-dependent warming
33 (Pepin et al., 2022) will likely change future ROS frequency (ROS fr) in snow-dominated regions (López-
34 Moreno et al., 2021). To date, research has been focused on the ROS predictability (Corripio and López-
35 Moreno, 2017), detection and validation methods through remote sensing (Bartsch et al., 2010) and models
36 (Serreze et al., 2021). Several works have examined ROS from the climatological point of view, by analyzing
37 ROS spatial-temporal patterns for Alaska (Crawford et al., 2020), Japan (Ohba and Kawase, 2020), Norway
38 (Pall et al., 2019; Mooney and Li, 2021) or the Iberian Peninsula mountains (Morán-Tejeda et al., 2019). ROS
39 events have also been linked with Northern-Hemisphere and Arctic low-frequency climate modes of variability
40 (Rennert et al., 2009; Cohen et al., 2015) as well as synoptic weather types (Ohba and Kawase, 2020). Further,
41 several works in mountain catchments of Switzerland (Würzer et al., 2016), Germany (Garvelmann et al.,
42 2014a), United-States (Marks et al., 1992), Canadian Rockies (Pomeroy et al., 2016) or Spain (Corripio and
43 López-Moreno, 2017), have portioned the contribution of Surface Energy Balance (SEB) components during
44 ROS events. ROS alters snow and soil conditions, since the liquid water percolation creates ice layers and
45 could alter the snowpack stability (Rennert et al., 2009). In severe ROS events, water percolation reaches the
46 ground, and the subsequent water freezing causes latent heat releases, leading to soil and permafrost warming
47 (Westermann et al., 2011). Positive heat fluxes during ROS events enhance snow runoff (Corripio and López-
48 Moreno, 2017), especially in warm and wet snowpacks (Würzer et al., 2016). ROS can also trigger a snow
49 avalanche in mountain zones (Conway and Raymond, 1993), flash flood events (Surfleet and Tullios, 2013),
50 impacts in tundra ecosystems (Hansen et al., 2013) and herbivore populations such as reindeers (Kohler and
51 Aanes, 2004).

52

53 Different ROS fr trends have been found since the last half of the 20st century. In the western United-States
54 and from 1949 to 2003 (McCabe et al., 2007) found a general ROS fr decrease in low elevations but an increase
55 in high elevations. Similarly, the analysis of six major German basins from 1990 to 2011, reveals an upward
56 (downward) ROS fr trend during winter (spring) at low and high elevations (Freudiger et al., 2014). On the
57 contrary, from 1979 to 2014, no winter ROS fr trends were found across the entire Northern-Hemisphere
58 (Cohen et al., 2015). ROS projections for the end of the 21st century suggest a general ROS fr increase in cold
59 regions. This is projected for Alaska (Bieniek et al., 2018), Norway (Mooney and Li, 2021), western United-
60 States (Musselman et al., 2018), Canada (il Jeong and Sushama, 2018) or Japan (Ohba and Kawase, 2020). In
61 European mid-latitude mountain ranges, such as the Alps, ROS fr is expected to increase (decrease) in high
62 (low) elevation sectors (Beniston and Stoffel, 2016; Morán-Tejeda et al., 2016). López-Moreno et al. (2021)
63 compared the ROS sensitivity to climate warming across 40 global basins and detected the highest ROS fr
64 decreases in low-elevated and warm Mediterranean mountain sites. Despite the increasing understanding of
65 ROS spatio-temporal past and future trends, little is known about the ROS sensitivity to climate warming



66 across southern European mountain ranges, such as the Pyrenees.

67

68 This work examines the ROS sensitivity to temperature and precipitation change (delta-change) for low (1500
69 m), mid (1800 m) and high (2400 m) elevations of the Pyrenees. ROS delta-change is analyzed using a
70 physically based snow model, forced with reanalysis climate data perturbed according to 21st century climate
71 projections spread for range (Amblar-Francés et al., 2020). Previous studies in alpine zones have shown
72 different ROS response to warming depending on the area and month of the season (e.g., Morán-Tejeda et al.
73 2016). For this reason, results are focused on these two factors. First, we analyze ROS drivers, namely height
74 of snow (HS) and snowfall fraction (Sf) (López-Moreno et al., 2021), sensitivity to temperature and
75 precipitation. Next, we examine ROS patterns and their response to warming by three key ROS indicators,
76 namely:

77

78 (a) Number of ROS days for a season (ROS fr).

79 (b) Average rainfall quantity during a ROS day (ROS rain).

80 (c) Average daily snow ablation during a ROS day (ROS ablation).

81

82 The study area is presented in Section 2. Section 3 describes the data and methods. Section 4 presents the
83 results. We finally discuss the anticipated ROS spatio-temporal changes, their socio-environmental impacts
84 and hazards in Section 5.

85

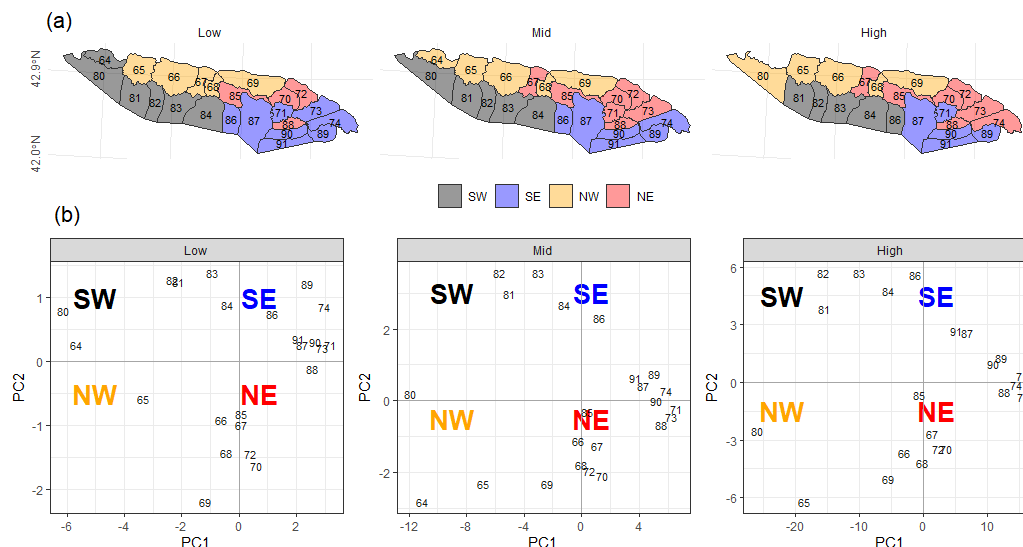
86 **2 Regional setting**

87

88 The Pyrenees mountain range is located between the Atlantic Ocean (West) and the Mediterranean Sea (East),
89 and is the largest (~ 450 km) mountain range of the Iberian Peninsula. Elevation increases towards the central
90 massifs, where the highest peak is found (Aneto, 3,404 m asl). Glaciers expanded during the Little Ice Age and
91 nowadays are located in the highest mountain summits (Vidaller et al., 2021). The regional annual 0 °C
92 isotherm is at ca. 2700 m (Del Barrio et al., 1990), and at ca. 1600 m during the cold season (López-Moreno
93 and Vicente-Serrano, 2011). The elevation lapse-rate is ca. 0.6°/100 m, being slightly lower during winter
94 (Navarro-Serrano and López-Moreno, 2017). Annual precipitation is ca. 1000 mm/year (ca. 1500 m);
95 maximum values are found in the northern-western massifs (around 2000 mm/year), decreasing towards the
96 southern-eastern (SE) area (Lemus-Canovas et al., 2019). Precipitation is predominantly (> 90%) solid above
97 1600 m from November to May (López-Moreno, 2005). Due to the mountain alignment, relief configuration,
98 and the distance to the Atlantic Ocean, seasonal snow accumulations in the northern slopes (ca. 500 cm/season),
99 almost doubles the recorded in the SE area for the same elevation (ca. 2000 m) (Bonsoms et al., 2021b). In the
100 western and central area of the southern slopes of the range (SW sector, Figure 1), snow accumulation is ruled
101 by Atlantic wet and mild flows, which are linked with negative North Atlantic Oscillation (NAO) phases (SW
102 and W synoptic weather types) (López-Moreno, 2005; Alonso-González et al., 2020b; Bonsoms et al., 2021a).
103 Positive Western Mediterranean Oscillation (WeMO) phases (NW and NE synoptic weather types) control the



104 snow patterns in the northern-eastern (NE) slopes of the range (Bonsoms et al., 2021a). Snow ablation starts
 105 in February (May) in low (high) elevations. The energy available for snow ablation is controlled by net radiation
 106 (55 %, over the total), latent (32 %) and sensible (13 %) heat fluxes (Bonsoms et al., 2022a).
 107



108

109

110 **Figure 1.** (a) Pyrenean massifs sectors (colors) for low, mid and high elevation. (b) Principle Component
 111 Analysis (PCA) scores of each massif for low, mid and high elevation. The black numbers are the SAFRAN
 112 massif's identity numbers defined by Vernay et al. (2022). Note that high elevation does not include massif
 113 number 64 since this massif does not reach 2400 m.

114

115 3 Data and methods

116

117 3.1 Snow model description

118

119 Snowpack is modeled using the energy and mass balance snow model FSM2 (Essery, 2015). The FSM2 was
 120 forced at hourly resolution for each massif and elevation range (c.f. Sect. 3.3) for the baseline climate (1980 –
 121 2019) and several climate perturbed scenarios (c.f. Sect. 3.4). Sf was quantified using a threshold-approach.
 122 Precipitation was snowfall when temperature was < 1 °C according to previous ROS research in the study zone
 123 (Corripio and López-Moreno, 2017) and the average rain-snow temperature threshold for the Pyrenees
 124 (Jennings et al., 2018). Snow cover is calculated by a linear function of snow depth, snow albedo is estimated
 125 based on a prognostic function with the new snowfall. Snow thermal conductivity is estimated based on snow
 126 density. Liquid water percolation is calculated based on a gravitational drainage. Compaction rate is simulated
 127 from overburden and thermal metamorphism. The atmospheric stability is estimated through the Richardson
 128 number stability functions to simulate latent and sensible heat fluxes. The selected FSM2 configuration



129 includes three snow layers and four soil layers. The detailed FSM2 physical parameters and Fortran
130 compilation numbers are shown in Table S1. The FSM2 model and configuration was previously validated in
131 the Pyrenees at Bonsoms et al. (2022b). FSM2 has been successfully used in snow model sensitivity studies in
132 alpine zones (Günther et al., 2019). FSM2 has been implemented in a wide range of alpine conditions, such as
133 for the Iberian Peninsula mountains (Alonso-González et al., 2019), Spanish Sierra Nevada (Collados-Lara et
134 al., 2020) or swiss forest environments (Mazzotti et al., 2020) snowpack modeling. FMS2 has been integrated
135 in snow data-assimilation schemes in combination with in-situ (Smyth et al., 2022) and remote-sensing data
136 (Alonso-González et al., 2022).

137

138 **3.2 Atmospheric forcing data**

139

140 The FSM2 was forced with the SAFRAN meteorological system reanalysis dataset for flat slopes (Vernay et
141 al., 2022). The SAFRAN meteorological system integrates meteorological simulations, remote-sensing cloud
142 cover data, and instrumental records through data-assimilation. SAFRAN is forced with a combination of
143 homogenized ERA-40 reanalysis (1958 to 2002) and the numerical weather prediction model ARPEGE (2002
144 to 2020). SAFRAN system was firstly designed for avalanche monitoring (Durand et al., 1999, 2009), but the
145 accurate results obtained enhanced the diffusion of the meteorological system and its integration in the French
146 hydrometeorological modelling system by the local weather service, Météo-France (Habets et al., 2008).
147 SAFRAN performance has been extensively validated. For instance, in long-term and high-resolution climate
148 analysis (Devers et al., 2021), seasonal forecasting (Ceron et al., 2010) or the meteorological modelling of
149 continental France (Quintana-Seguí et al., 2008) and Spain (Quintana-Seguí et al., 2017). SAFRAN system
150 has been used as meteorological forcing data for the snow modeling in complex alpine terrain (Revuelto et al.,
151 2018; Deschamps-Berger et al., 2022), to study long-term snow evolution (Réveillet et al., 2022), avalanche
152 hazard forecasting (Morin et al., 2020), snow climate projections (Verfaillie et al., 2018), snow depth (López-
153 Moreno et al., 2020) and energy heat fluxes spatio-temporal trends (Bonsoms et al., 2022a). SAFRAN
154 meteorological system exhibit and accuracy of around 1 °C in air temperature and around 20 mm in the monthly
155 cumulative precipitation (Vernay et al., 2022).

156

157 **3.3 Spatial areas**

158

159 SAFRAN system provides data at hourly resolution from 0 to 3600 m, by steps of 300 m, grouped by massifs.
160 The SAFRAN massifs (polygons of Figure 1) were chosen for their relative topographical and climatological
161 similarities (Durand et al., 1999). We selected the 1500 m (low), 1800 m (mid), and 2400 m (high) specific
162 elevation bands of the Pyrenees. In order to retain the main spatial differences across the mountain range,
163 reduce data dimensionality and include the maximum variance, massifs with similar interannual snow
164 characteristics were grouped into sectors by performing a Principal Component Analysis (PCA). PCA is an
165 extensively applied statistical method for climatological and snow spatial regionalization (i.e., López-Moreno
166 and Vicente-Serrano, 2007; Schöner et al., 2019; Alonso-González et al., 2020a; Matiu et al., 2021; Bonsoms



167 et al., 2022a). A PCA was applied over HS data for all months and years of the baseline climate. Massifs were
168 grouped into four groups depending on the maximum correlation to the first (PC1) and second (PC2) scores.
169 Pyrenean sectors were named South-West (SW), South-East (SE), North-West (NW) and North-East (NE) due
170 to their geographical position. Figure 1 shows the resulting Pyrenean regionalization for low, mid and high
171 elevation as well as the SAFRAN massifs PC1 and PC2.

172

173 **3.4 Sensitivity analysis**

174

175 ROS season extension was defined according to ROS occurrence during the baseline climate period. For the
176 purposes of this research, seasons are classified as follows: October and November (Autumn); December,
177 January, and February (Winter); March, April, May, and June (Spring); and July (Summer). August and
178 September are not included due to the absence of regular snow cover. ROS sensitivity to precipitation, air
179 temperature, increasing incoming longwave radiation (LWin) accordingly, was performed through a delta-
180 change approach. This method has been successfully applied and validated for analyzing the snow sensitivity
181 to temperature and precipitation changes in many mountains, such as the Pyrenees (e.g., López-Moreno et al.,
182 2013), the Iberian-Peninsula mountain areas outside the Pyrenees (Alonso-González et al., 2020a), Alps (Marty
183 et al., 2017), Canadian basins (Pomeroy et al., 2015; Rasouli et al., 2019), or western United-States
184 (Musselman et al., 2017b), among other works. Delta-change has also been also performed in global ROS
185 sensitivity to temperature change studies (López-Moreno et al., 2021). SAFRAN reanalysis climate data was
186 perturbed according to Spanish Meteorological Agency climate change scenarios projected for the 21st
187 Century in the Pyrenees (Amblar-Francés et al., 2020). Precipitation was increased (+10%), left unchanged
188 (0 %) and decreased (-10%). Air temperature was perturbed from +1°C to +4°C by +1°C. LWin was increased
189 due to warming, by applying the Stefan-Boltzmann law, using the Stefan-Boltzmann constant, and the hourly
190 atmospheric emissivity derived from SAFRAN air temperature and LWin.

191

192 **3.5 HS, Sf and ROS climate indicators**

193

194 The average HS and Sf delta-change (expressed in % per °C) is the average seasonal HS and Sf anomalies
195 under the baseline climate and divided by degree of warming. Days are classified as ROS days when daily
196 rainfall amount was ≥ 10 mm and HS ≥ 0.1 m, according to previous works (Musselman et al., 2018; López-
197 Moreno et al., 2021). ROS fr are the number of ROS days. ROS rain is the average daily rainfall (mm) during
198 a ROS day. ROS ablation is the average daily snow ablation (cm) during a ROS day. The average daily snow
199 ablation is the daily average HS difference between two consecutive days (Musselman et al., 2017a). Only the
200 days when a negative HS difference occurred were selected. ROS exposure is the relation between ROS rain
201 (y-axis) and ROS fr (x-axis) differences from the baseline climate scenario for the massifs were ROS fr is
202 recorded for all increments of temperature.

203

204 **4 Results**



205

206 We provide an analysis of ROS drivers, near-present ROS patterns and their response to warming. ROS spatio-
207 temporal dynamics are analyzed by frequency, rainfall quantity and snow ablation. Since we have detected a
208 non-linear and counter-intuitive ROS sensitivity to temperature, ROS indicators values are shown for each
209 increment of temperature, grouped by elevation and sectors, namely SW, SE, NW and NE.

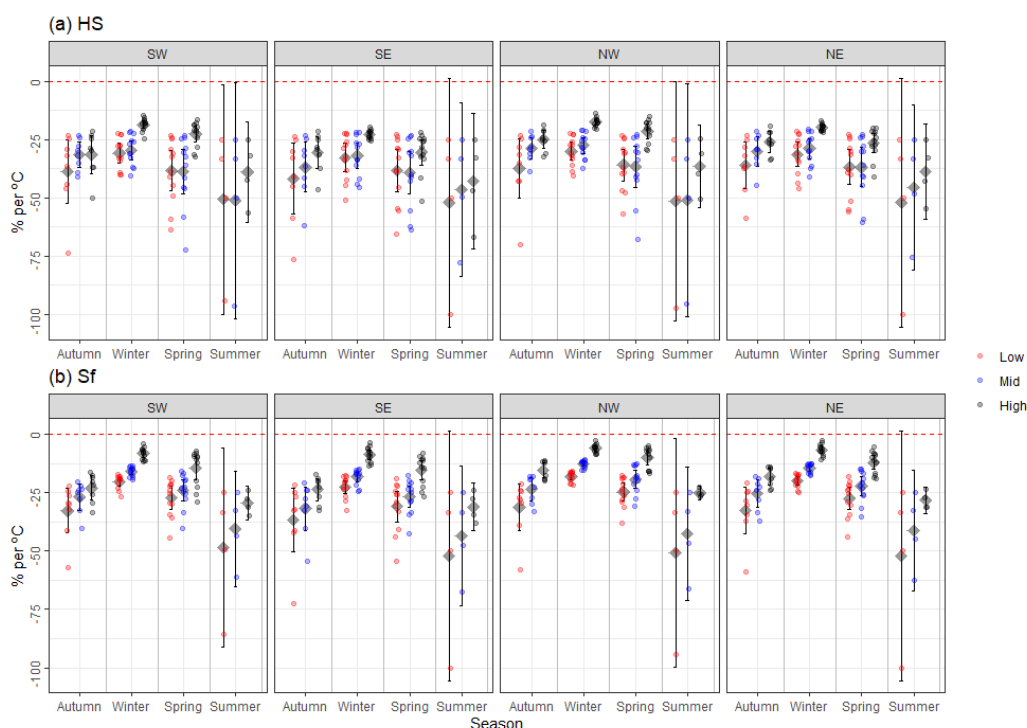
210

211 **4.1 ROS drivers**

212

213 HS and Sf delta-change is shown in Figure 2. Seasonal HS and Sf delta-change variability is mostly controlled
214 by the increment of temperature, season, elevation, and spatial sector (Figure S1). The role of precipitation
215 variability in the seasonal HS evolution is moderate to low (Figure S2 to S4). Only in high elevation an upward
216 trend of precipitation (at least > 10%) can counterbalance small increments of temperature (< 1°C, over the
217 baseline climate) from December to February (Figure S4). For this reason, precipitation was excluded to further
218 analysis. Snow in low and mid elevations during summer is rarely observed, however, marginal snow cover in
219 high elevation can last until June and July, especially in the wettest sectors of the range (NW and SW). Seasonal
220 HS and Sf delta-change show an elevation-dependent pattern to warming and large seasonality. The average
221 HS decrease per °C ranges from 39 %, 37 % and 28 % per °C, for low, mid and high elevations, respectively.
222 However, relevant differences are found depending on the season and degree of warming (Figure 2). Maximum
223 HS and Sf reductions are found in low and mid elevations during the shoulders of the season (autumn and
224 spring), coinciding with the time when ROS events are more frequent for the baseline climate (Figure 3). In
225 these elevations, maximum HS decreases (52 % over the baseline climate) are modeled for spring when
226 temperature is + 1°C. The greatest HS decreases in high elevation areas are modeled for summer (54 % HS
227 decrease for 1°C). If temperature reaches maximum values (+ 4 °C), seasonal HS is reduced 92 %, 89 %, and
228 79 % for low, mid, and high elevations, respectively (Figure S5).

229



230

231

232 **Figure 2.** Seasonal (a) HS and (b) Sf anomalies over the baseline climate. Data are shown by elevation
 233 (colors), season (x-axis) and sectors (boxes). Points represent the average seasonal HS and Sf anomalies
 234 grouped by month of the season and increment of temperature (from 1°C to 4°C). The black diamond point
 235 indicates the mean, whereas the upper and lower error bars show the Gaussian confidence based on the
 236 normal distribution.

237

238 Sf shows lower sensitivity to warming than HS and maximum reductions in autumn. On average, Sf decreases
 239 by 29%, 22 %, and 12 % per °C for low, mid, and high elevations, respectively. An increase of 4°C supposes
 240 Sf reductions of 80 %, 69 % and 49 % for low, mid, and high elevations. HS and Sf delta-change shows also
 241 different sensitivities across the range. Independently of the elevation band and season, the SE exhibit the
 242 greatest HS and Sf decreases (41 % and 35 % per °C, respectively). On the contrary, minimum reductions are
 243 expected in the northern slopes (NW and NE).

244

245 4.2 ROS frequency

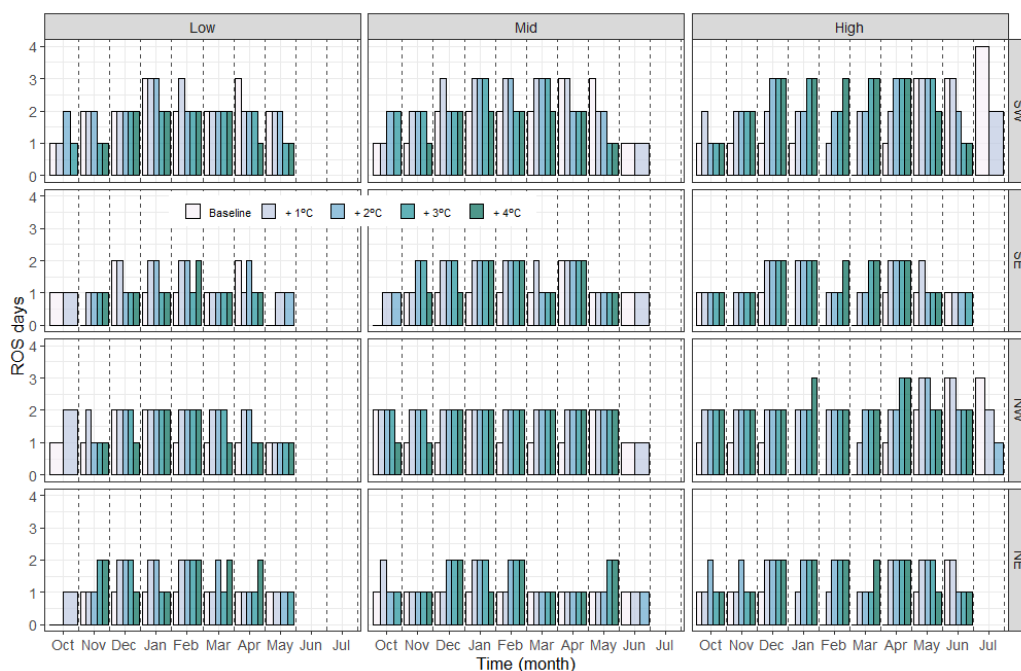
246

247 Low elevation annual ROS fr for the baseline climate is 17, 8, 10 and 7 days/year for SW, SE, NW, NE sectors,
 248 respectively (Figure 3). The highest annual ROS fr is however observed at mid elevation. Here, annual ROS
 249 fr is 17, 9, 12 and 9 for SW, SE, NW, NE sectors. Within these elevations, the maximum ROS fr is detected in
 250 SW during winter and spring (7 days/season, for both elevations and seasons). The eastern Pyrenees follow a



251 similar seasonality. Maximum ROS fr in low elevation is found in winter (4 and 3 days/season, SE and NE,
 252 respectively), and during spring in mid elevation (4 and 3 days, SE and NE, respectively). ROS is rarely
 253 observed in SE during the latest month of spring (May), which contrast with the modeled values for SW (2
 254 and 3 days/month, for low and mid elevations, respectively). High elevation shows the minimum ROS fr. Here,
 255 comparisons between seasons reveal maximum ROS fr during summer, especially in SW (7 days/season),
 256 followed by NW (6 days/season), and NE (2 days/season).

257



258

259 **Figure 3.** ROS fr for baseline climate period and increments of temperature, grouped by months (x-axis),
 260 sector (rows) and elevation (columns).

261

262

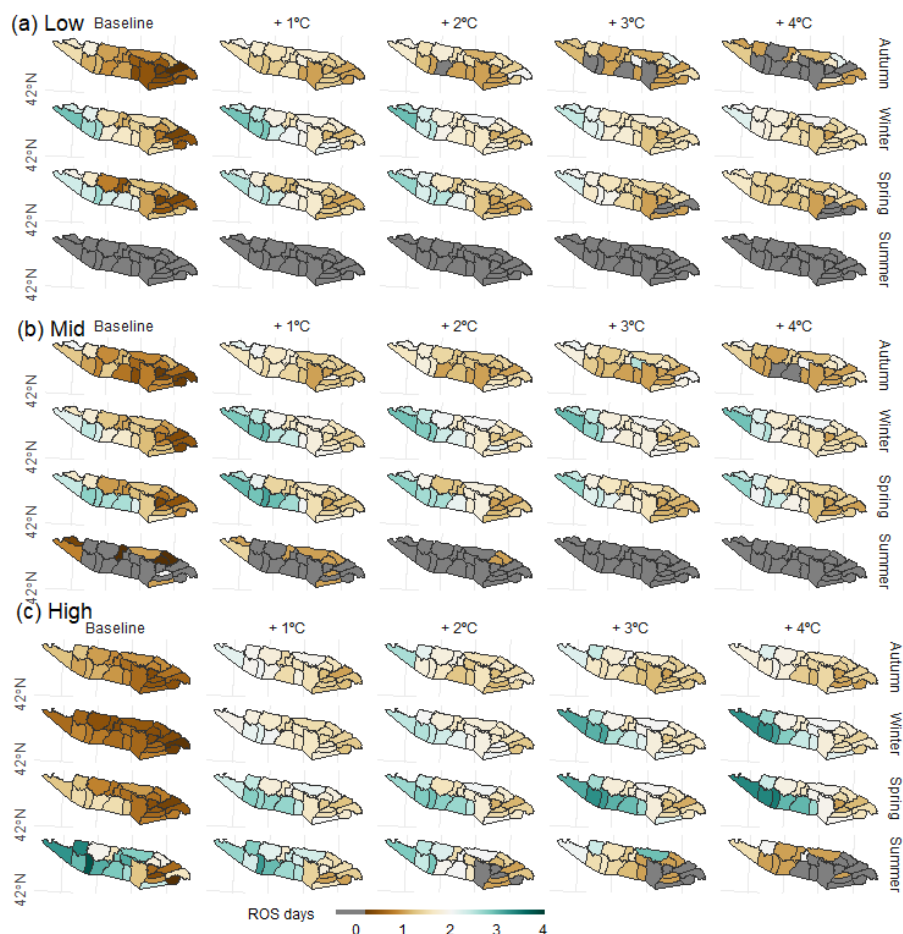
263 ROS fr response to warming vary depending on the month, increment of temperature, elevation, and sector.
 264 ROS tends to disappear in October for low elevations except in SW (Figure 3). The highest increases are seen
 265 during the winter for increments temperature lower than 3°C, particularly in NE, where ROS fr increases 1 day
 266 per month over the baseline scenario for + 1°C. In mid elevation, ROS fr increases in all regions from
 267 November to February (around 1 day per month, for + 1°C up to + 3°C). Similar increases are expected in NW
 268 and SW during the earliest months of spring and for low to moderate increments of temperature. The contrary
 269 is observed during the latest months of spring in SW, where warming reduces ROS events. A slight ROS fr
 270 increase is found during spring for the rest of the sectors (Figure 4). ROS events in June are expected to
 271 disappear for temperature increases higher than 1°C. Finally, high elevation shows the largest ROS fr variations
 272 (around 1 day/month for + 1°C). Maximum ROS fr increases (3 days/month) are found in SW for more than +



273 3°C. ROS fr progressively increases in March and April for all sectors but tends to decrease in May (for + 3°C),

274 June and July (for + 1°C).

275



276

277

278 **Figure 4.** Average ROS fr (days) for a season for (a) low, (b) mid and (c) high elevation. Data are shown for
 279 the baseline climate period and increment of temperature (left to right).

280

281 **4.3 ROS rain**

282

283 The spatial and temporal distribution of ROS rain is presented in Figure 5 and 6. The average low elevation
 284 ROS rain by year is 23, 28, 21, and 20 mm/day for SW, SE, NW, NE sectors, respectively. Similarly, the highest
 285 values in mid elevation are found in SE (29 mm/day, respectively). SE sector experiences the highest ROS rain
 286 during autumn and summer (around 40 mm/day in low and mid elevations). High elevation maximum ROS
 287 rain values are however found in the western Pyrenees during the onset and offset snow season. Here, the

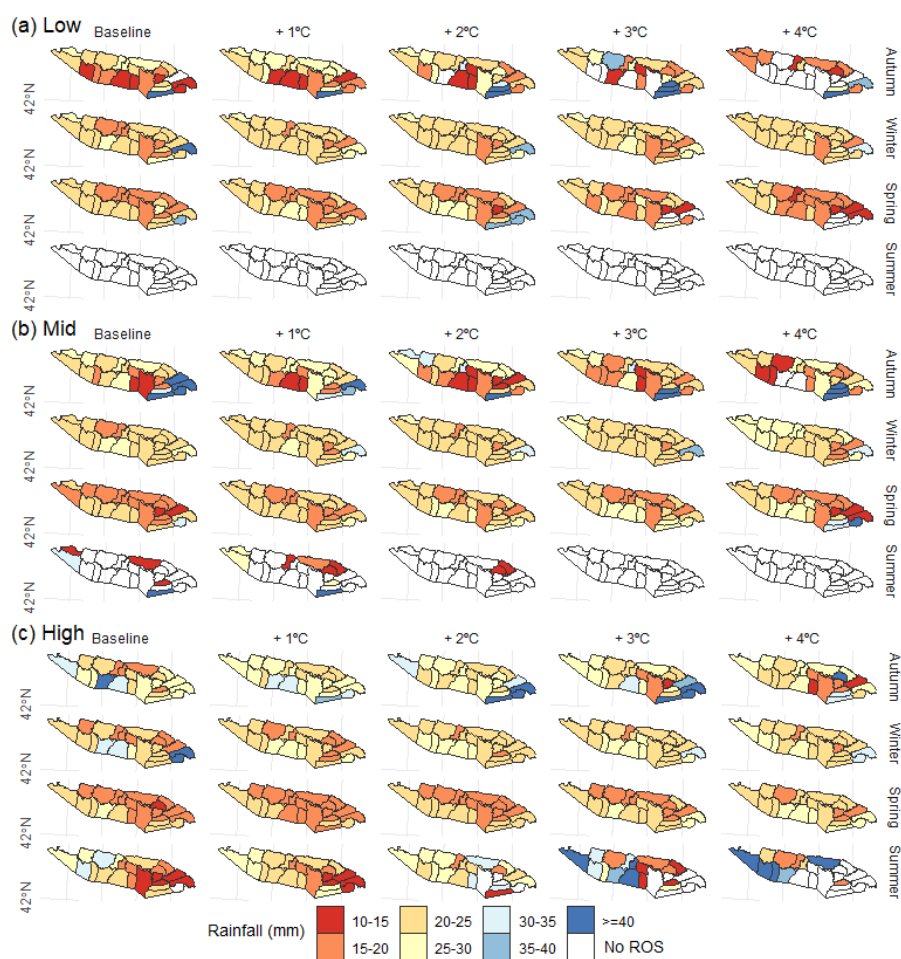


288 largest ROS rain spatial and seasonal distribution ranges from SW (29 mm/day, autumn), NW (28 mm/day,
 289 summer), SE (24 mm/day, autumn) to NE (23 mm/day, autumn).
 290



291
 292 **Figure 5.** ROS rain (mm) temporal evolution for baseline climate and increment of warming (colors),
 293 grouped by elevation (columns) and sector (rows).

294
 295 ROS rain progressively increases due to warming (4%, 4%, and 5% per °C for low, mid, and high elevations,
 296 respectively; Table S2). Small differences are found by elevation and sector. Low elevation ROS rain increases
 297 until + 3°C, and generally decreases for + 4°C during the earliest (October to December) and latest (April and
 298 May) months of the snow season. Similar patterns are found in mid elevation. ROS rain increases up to + 4°C,
 299 except in the SE sector for specific months (Figure 5). The latest sector shows also maximum ROS rain values
 300 in autumn due to torrential rainfall. High elevation ROS rain increase at a constant rate of around 5 % per °C.
 301 Yet, maximum increases are modeled in SW during summer, when ROS rain almost doubles the baseline
 302 climate (+ 40% for + 4°C).
 303



304

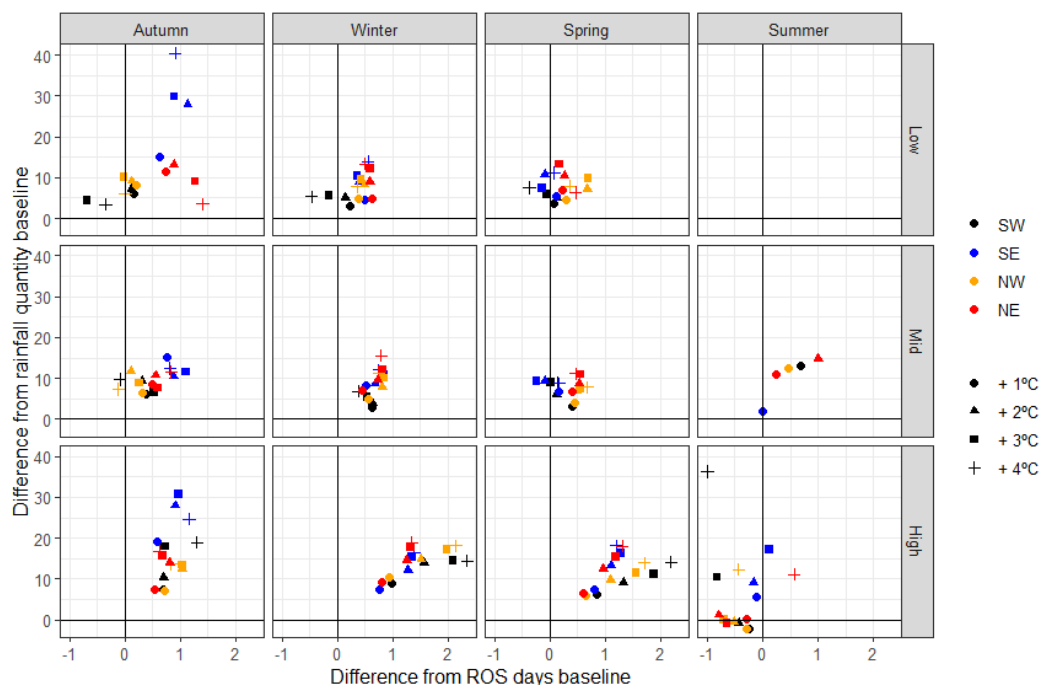
305

306 **Figure 6.** Average ROS rain (mm) for a season for (a) low, (b) mid and (c) high elevation. Data are shown
 307 for the baseline climate period and increment of temperature (left to right).

308

309 Data suggest that ROS exposure generally increases for all elevations and sectors during winter (except in SW
 310 for temperatures greater than 3°C). Nonetheless, remarkable spatial and seasonal differences are found. SE
 311 show the maximum values in autumn. On the contrary, small changes in frequency are detected in SW and
 312 NW, despite ROS rain is expected to increase (< 10mm/day). For the majority of sectors and elevations, ROS
 313 exposure generally increases in winter and spring. The minimum differences between sectors are detected in
 314 these seasons. In summer, ROS exposure tends to generally decrease for all elevations under severe warming
 315 due to snow cover depletion.

316



317

318 **Figure 7.** Average ROS exposure. Points are obtained by a scatterplot between ROS rain difference from
 319 baseline climate (y-axis) and ROS days difference from baseline climate (x-axis). Data is calculated by the
 320 average difference between (a) the baseline scenario and (b) the different perturbed scenarios, only for the
 321 massifs where ROS fr exists on (a) and (b). Data are shown for each season (columns), elevation (rows),
 322 sector (color) and increment of temperature (point shape).

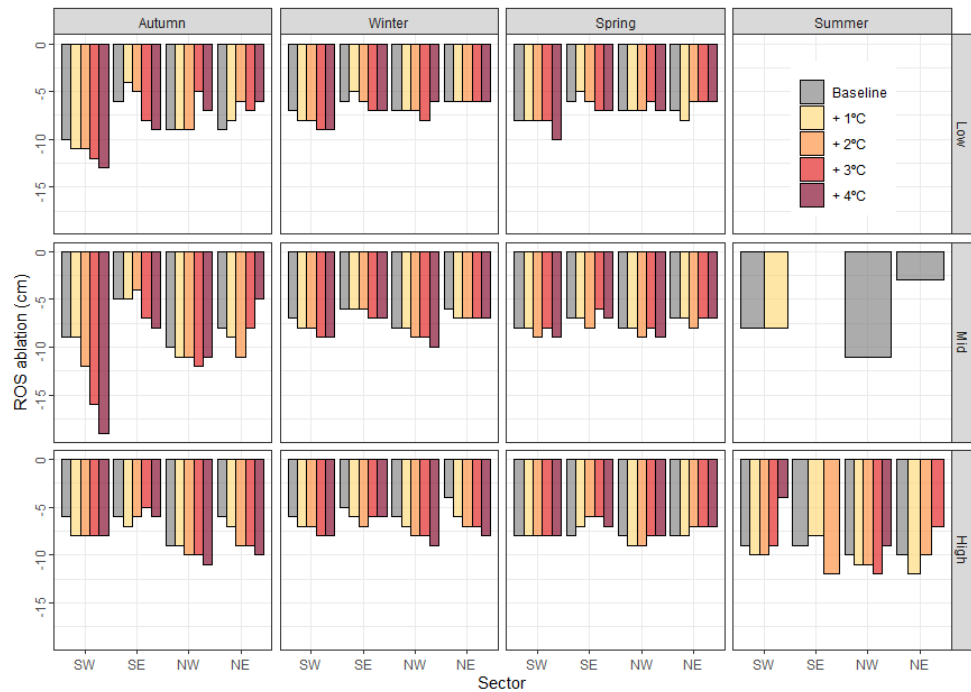
323

324 4.4. ROS ablation

325

326 ROS ablation is presented at Figure 8 and 9. ROS ablation ranges from -10 cm/day in NW high elevation
 327 (summer) to - 5 cm/day in NE high elevation (winter). ROS ablation nearly doubles the average daily snow
 328 ablation for all days on a season (Figure S6). Comparison with the reference baseline period reveals contrasting
 329 ROS ablation changes depending on the season, elevation and sector. Overall ROS ablation progressively
 330 increases due to warming in coldest zones and months of the season. The largest ROS ablation increments are
 331 detected in autumn and winter. For the former, ROS ablation increases at a generally constant rate in SW (11 %
 332 NE (19 %) and NW (4 % per °C). For the latter, ROS ablation increases also in SW (11 %), NW (14 %) and
 333 NE (34 % per °C). In detail, maximum ROS ablation due to warming is found for mid elevation during autumn
 334 (Figure 8). ROS ablation exhibit slow and no-changes in the warmest zone (SE), as well in the warmest months
 335 of the season, regardless the elevation band.

336



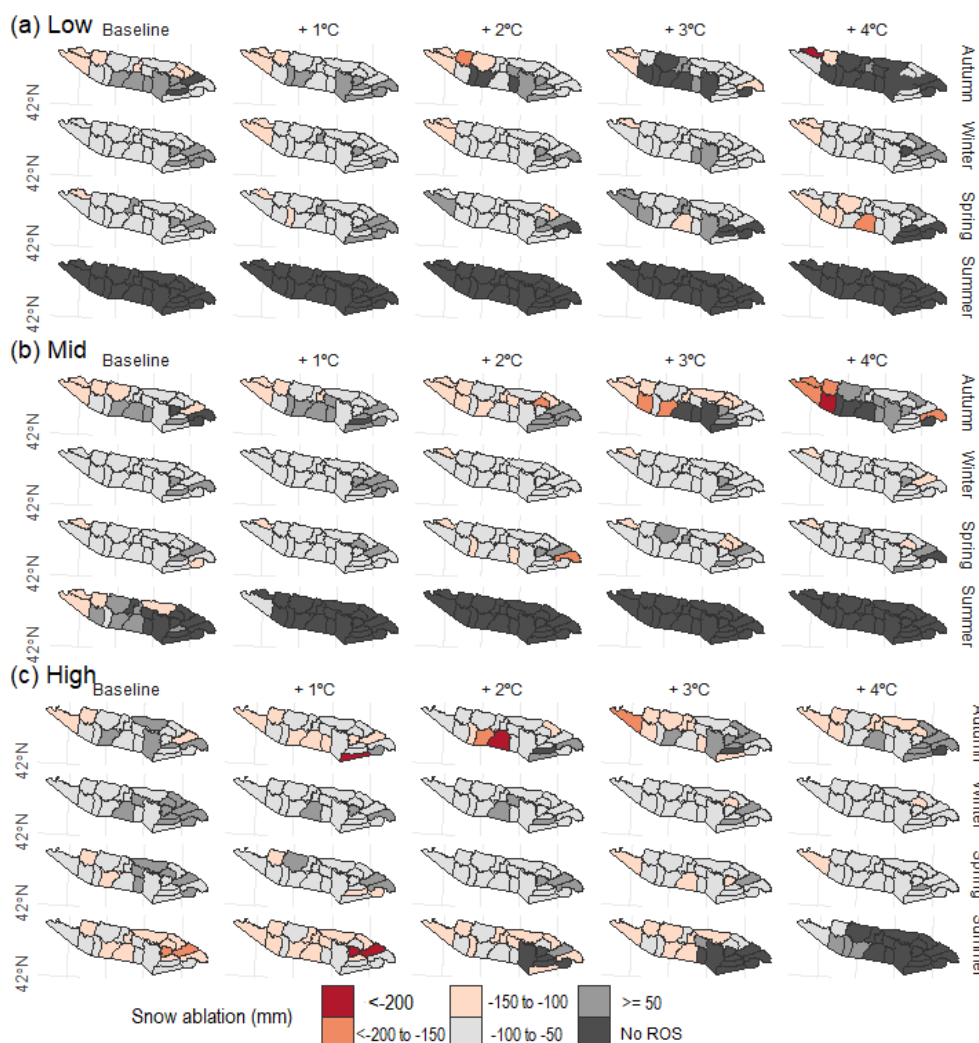
337

338

339 **Figure 8.** ROS ablation (y-axis) for baseline climate period and increment of temperature (colors), sector (x-
340 axis), season (columns) and elevation (rows).



341



342

343

344 **Figure 9.** Average ROS ablation for a season for (a) low, (b) mid and (c) high elevation. Data are shown for
 345 the baseline climate period and increment of temperature (left to right).

346

347 **5 Discussion**

348

349 The Pyrenees experienced a statistically significant positive temperature trend since the 1980s (ca. + 0.2
 350 °C/decade) but no statistically significant precipitation trends are detected (OPCC, 2018) due to strong spatial
 351 (Vicente-Serrano et al., 2017), inter-annual and long-term variability of the latter (Peña-Angulo et al., 2021).
 352 Depending on the study period different snow trends were found. From ca. 1980 to 2010, non-statistically



353 significant snow days and snow accumulation positive trends were generally detected at > 1000 m (Buisan et
354 al., 2016), 1800 m (Serrano-Notivoli et al., 2018), and > 2000 m (Bonsoms et al., 2021a). Long-term trends
355 (1957 to 2017), however, reveal statistically-significant snow depth decreases at 2100 m, but large variability
356 depending on the sector and the snow indicator (López-Moreno et al., 2020). Climate projections for the end
357 of the 21st century suggest an increase of temperature (> 3°C), together with low precipitation shifts (< 10%)
358 from autumn to spring (Amblar-Francés et al., 2020). Within this climate context, ROS spatio-temporal
359 patterns will likely change. In order to anticipate future scenarios, ROS sensitivity to warming was analyzed
360 through three key indicators of frequency, rainfall intensity and snow ablation.

361

362 **5.1 ROS spatial variability**

363

364 The climatic setting of the Pyrenees as well as its relief configuration determines a remarkable spatial and
365 temporal variability of ROS events. The contradiction between rainfall ratio increases and snowpack
366 reductions, as well as the high spatial and monthly differences found, explain the complex ROS response to
367 warming. HS decrease by 39 %, 37 % and 28 % per °C, for low, mid and high elevations, respectively.
368 Similarly, Sf decreases by 29 %, 22 %, and 12 % per °C for low, mid, and high elevations, respectively,
369 providing evidence of an elevation-dependent snow sensitivity to temperature change. HS and Sf maximum
370 reductions are reached for 1°C of warming, suggesting non-linear HS decreases, in accordance with previous
371 snow sensitivity to climate change reported in central Pyrenees (López-Moreno et al., 2013). In detail, SW and
372 NW annual ROS fr almost doubles (17 and 12 days/year, respectively) the one recorded in SE and NE (9
373 days/year, for both sectors). Maximum ROS fr for a season are found in SW and NW because of larger snow
374 magnitudes in this sector (i.e., López-Moreno, 2005; López-Moreno et al, 2007; Navarro-Serrano et al., 2017;
375 Bonsoms et al., 2021a). Thus, snow cover last longer until spring when minimum Sf values are found (Figure
376 S1). This sector is the most exposed to SW and W air flows (negative NAO phases) (López-Moreno, 2005),
377 which bring wet and mild conditions over the mountain range, leading to most ROS-related floods in the range
378 (Morán-Tejeda et al., 2019). The generally ROS rain increase reported in this work (independently of the
379 increment of temperature and elevation) is explained by the Sf reduction expected for all sectors (Figure 2).
380 Maximum ROS rain is generally detected in spring (May), except in NE high elevation zones and SE (all
381 elevations). In the latter sectors, ROS rain tends to dissappear in October under large (> 2°C) increments of
382 temperature. The seasonal snow accumulation in NE and SE is lower-than-average due to the lower influence
383 of Atlantic climate in these sectors of the range. Hence, large increments of warming decreases ROS fr due to
384 snow cover depletion in early autumn and late spring (Figure S1). In addition, SE is closer to the 0°C due to
385 higher-than-average sublimation, latent and radiative heat fluxes (Bonsoms et al., 2022a) and for this reason
386 in this sector each increment of temperature has larger effects on the Sf, HS and ROS fr reduction (Figure 2).
387 High elevation show the largest variation over the baseline climate as well as ROS exposure because of the
388 larger snowpack magnitude and duration compared to low and mid areas. Thus, high elevation snow duration
389 last until spring and summer, when the largest shift from snowfall to rainfall is found. On the other hand, mid
390 elevation shows the maximum ROS rain since the amount of moisture for condensation decreases while air



391 masses increase height (Roe and Baker, 2006). Furthermore, the largest ROS rain is detected in SE during
392 autumn (Figure 6), because of the exposure of this region to Mediterranean low-pressure systems (negative
393 WeMO phases), that usually trigger heavy rainfall events during this season (Lemus-Canovas et al., 2021).

394

395 **5.2 ROS temporal evolution**

396

397 Recent ROS trends in other mid-latitude areas are in accordance with ROS analysis presented here. Freudiger
398 et al. (2013) analyzed the ROS trends (1950–2011 period) of the Rhine, Danube, Elbe, Weser, Oder, and Ems
399 (Central Europe) basins. They found an overall ROS fr increase during January and February (1990 to 2011
400 period), which is consistent with the ROS rain and frequency increase detected in winter for the Pyrenees for
401 all elevations and increment of temperature. Similarly, in Sitter River (NE Switzerland), a ROS fr increase of
402 around 40% (200%) at <1500 m (>2500 m) was detected between 1960 and 2015 (Beniston and Stoffel, 2016).
403 During the last half of the 20th century, ROS fr trends show an upward (downward) trend in high (low) elevation
404 in western United-States (McCabe et al., 2007), as well as in southern British Columbia (Loukas et al., 2002)
405 and at catchment scale in Oregon (United-States) (Surfleet and Tullos, 2013). Same ROS fr increases
406 (decreases) has been detected from 1980 to 2010 in Norwegian high (low) elevated mountain zones (Pall et
407 al., 2019). However, in contradiction with our results and previous studies, winter Northern-Hemisphere ROS
408 fr trends (1979-2014 period) show no-clear trends (Cohen et al., 2015).

409

410 Results exposed in this work provide more evidence of ROS fr increases in high-elevation zones, as it has been
411 suggested by climate projections and ROS sensitivity to temperature studies. ROS show an elevation-
412 dependent pattern that was previously reported in the Swiss Alps (Morán-Tejada et al., 2016). In Sitter River
413 (NE Switzerland), an increase of 2 to 4 °C over the 1960 to 2015 period results in an increase of the ROS fr
414 by around 50% at > 2500 m (Beniston and Stoffel, 2016). Likewise, 21st century high-emission scenarios
415 (RCP8.5), suggest increases in ROS fr and intensity in Gletsch (Switzerland) high-elevation area; however, on
416 climate projections for ROS definitions that include snow melting (Musselman et al., 2018), natural climate
417 variability contributes to a large extend (70 %) of ROS variability (Schirmer et al., 2022). Li et al. (2019)
418 analyzed the future ROS fr in the conterminous United-States and detected a nonlinear trend ROS due to
419 warming, which is consistent with the different ROS rain and frequency responses depending on the increment
420 of temperature detected in our work. Climate projections for the mid-end of the 21th century projected positive
421 ROS fr and rainfall trends in Western United-States and Canada (il Jeong and Sushama, 2018). Similarly, ROS
422 fr will likely decrease (increase) in the warmest months of the season in low (high) elevation areas of western
423 United-States (Musselman et al., 2018). The same is projected Norwegian mountains (Mooney and Li, 2021).
424 López-Moreno et al. (2021) analyzed 40 worldwide basins ROS sensitivity to warming. In their study they
425 found a decrease of ROS events in warm mountain areas. However, they detected ROS fr increases in cold-
426 climate mountains where large snow accumulation is found despite warming. In accordance with our results,
427 they identified large seasonal differences and ROS fr decreases in Mediterranean mountains due to snow cover
428 depletion in the lasts months of the snow season.



429

430 **5.3 ROS ablation**

431

432 Warming increases ROS ablation from autumn to winter on deep snowpacks and in the coldest sectors of the
433 range, due to higher energy for snow ablation and closer 0°C isotherm conditions in a warmer than baseline
434 climate. Nevertheless, data show low or decreases in ROS ablation in SE and spring, since the snowpack is
435 already near to the isothermal conditions. These results go in line with results modelled for cold and warm
436 Pyrenean sites (López-Moreno et al., 2013) as well as for different Northern-Hemisphere sites (Essery et al.,
437 2020). ROS ablation indicator is also indirectly affected by the HS magnitude decreases (30 % per °C; Figure
438 2), and therefore lower ROS ablation is directly affected by lower HS magnitudes. Previous literature pointed
439 out that warming have counter-intuitive effects on snow ablation patterns. Higher than average temperatures
440 advance the peak HS date on average 5 days per °C in mid and high elevations (Bonsoms et al., 2022b),
441 triggering earlier snow ablation onsets, and therefore lower solar radiation fluxes (López-Moreno et al., 2013;
442 Lundquist et al., 2013; Pomeroy et al., 2015; Musselman et al., 2017a; Sanmiguel-Vallelado et al., 2022), as
443 well as earlier snow depletion before the maximum advection of heat fluxes into the snowpack (spring)
444 (Bonsoms et al., 2022a). Slower snow melt rates in a warmer climate have been detected in Western United-
445 States (Musselman et al., 2017), as well as the entire Northern-Hemisphere (Wu et al., 2018). Low or inexistent
446 changes in snow ablation on warm and marginal snowpacks has been previously detected in the central
447 Pyrenees (López-Moreno et al., 2013), in forest and open areas (Sanmiguel-Vallelado et al., 2022), in the entire
448 range (Bonsoms et al., 2022b), and other Iberian Peninsula Mountain ranges outside the Pyrenees (Alonso-
449 González et al., 2020a).

450 ROS ablation is larger than the average snow ablation during a snow ablation day (Figure S6) due to higher
451 SEB positive fluxes. Several works analyzed SEB changes on ROS events, and different SEB contributions
452 has been found depending on the geographical area (Mazurkiewicz et al., 2008; Garvelmann et al., 2014b;
453 Würzer et al., 2016; Corripio and López-Moreno, 2017; Li et al., 2019), ranging from net radiation in Pacific
454 North West (Mazurkiewicz et al., 2008) to LWin and turbulent heat fluxes in conterminous United-States
455 mountain areas (Li et al., 2019) or the Swiss Alps (e.g., Würzer et al., 2016). In general, studies in mid-latitude
456 mountain ranges have shown that turbulent heat fluxes contribute between 60 and 90 % of the energy available
457 for snow ablation during ROS days (e.g., Marks et al., 1998; Garvelmann et al. 2014; Corripio and López-
458 Moreno, 2017). In the central Pyrenees (> 2000 m) the meteorological analysis of a ROS event reveals that
459 ROS ablation is larger than a normal ablation day because of the large advection of LWin and especially
460 sensible heat fluxes (Corripio and López-Moreno, 2017). LWin increases due to the high cloud cover and warm
461 air, as it is frequently observed during ROS episodes (Moore and Owens, 1984).

462



463 **5.4 ROS socio-environmental impacts and hazards**

464 Temperature-induced changes in the seasonal snowpack and during ROS days suggest several hydrological
465 shifts including, but not limited to, earlier peak flows on the season (Surfleet and Tullos, 2013), rapid
466 streamflow peaks during high precipitation events in frozen soils (Shanley and Chalmers, 1999), faster soil
467 moisture depletion and lower river discharges in spring due to earlier snow melt in the season (Stewart, 2009).
468 The shortening of the snow season due to warming reported in this work will potentially alter alpine
469 phenological patterns (i.e., Wipf and Rixen, 2010) and expand forest cover (Szczypta et al., 2015). Although
470 vegetation branches intercepts a large amount of snowfall, intermediate and high vegetation shields short-wave
471 radiation, reduces snow wind-transport and turbulent heat fluxes (López-Moreno and Latron, 2008;
472 Sanmiguel-Valellado et al., 2022). Snow-forest interactions, their sensitivity to climate change as well as the
473 ROS hydrological response within a changing landscape is far from understood across the range and should be
474 the base of forecoming works.

475

476 The higher ROS exposure (Figure 7) will likely imply an increase of ROS-related hazards and impacts in the
477 mountain ecosystem. Heavy ROS rain changes snow metamorphism on saturated snowpacks and leads to
478 high-speed water percolation (Singh et al., 1997). The subsequent water refreezing changes the snowpack
479 conditions and creates an ice-layer in the snowpack that can reach the surface (Rennert et al., 2009). ROS can
480 cause plant damage (Bjerke et al., 2017) and the ice encapsulation of vegetation in tundra ecosystems can
481 trigger severe wildlife impacts, such as vertebrate herbivores starvation (Hansen et al 2013), reindeer
482 population mortality (Kohler and Aanes, 2004) and higher competition between species (Hansen et al 2014).
483 Nevertheless, any study to the date analyzed ROS-related impacts in flora and fauna across Southern-European
484 mountains. Snow albedo decay due positive heat fluxes and rainfall in ROS events (Corripio and López-
485 Moreno, 2017), lead to faster snow ablation even on the next days (e.g., Singh et al. 1997). The combination
486 of changes in internal snowpack processes, larger ROS rain, and more energy to ablate snow during spring
487 could enhance snow runoff, especially during warm and wet snowpack conditions (Würzer et al., 2016). In
488 snow-dominated regions ROS can lead to a specific type of avalanching (Conway and Raymond, 1993) and
489 floods (Surfleet and Tullos, 2013). The latter are the most environmental damaging risk in Spain (Llasat et al.,
490 2014) and around 50% of the flood in the Iberian Peninsula are due to ROS events (Morán-Tejeda et al., 2019).
491 More than half of the historical (1940 to 2012) flood events in the Ésera river catchment (central Pyrenees)
492 occurred during spring (Serrano-Notivoli et al., 2017), which coincides with the snow ablation season. ROS
493 floods have also economic impacts. For instance, a ROS flood event that occurred on 13th June of 2013 in the
494 Garonne River (Val d'Aran, central Pyrenees) cost approximately 20 million of euros to the public insurance
495 (Llasat et al., 2014).

496

497 **6 Conclusions**

498 The expected decreases in Sf and HS due to climate warming will likely change ROS spatio-temporal patterns



499 across the Pyrenees. Therefore, a better understanding of ROS is required. This work analyzed the ROS
500 sensitivity to warming by forcing a physically based snow model with perturbed reanalysis climate data (1980-
501 2019 period) for low, mid and high elevation areas of the Pyrenees. ROS delta-change is evaluated by
502 frequency, rainfall intensity and snow ablation during ROS days.

503 During the baseline climate period, annual ROS fr totals on average 10, 12 and 10 day/season for low, mid and
504 high elevations. Higher-than-average annual ROS fr are found in mid elevation SW (17 days/year) and NW
505 (12 days/year), which contrast with the minimums detected in SE (9 days/year). The different spatial and
506 seasonal ROS response to warming suggest that contrasting and shifting trends could be expected in the future.
507 Overall ROS fr decreases during summer in high elevation for $> 1^{\circ}\text{C}$. When temperature is progressively
508 increased the greatest ROS fr increases are found for SW high elevation (around 1 day/month for $+ 1^{\circ}\text{C}$). ROS
509 fr is highly sensitive to warming in the snow onset and offset months, when counterintuitive factors play a
510 key role. On the one hand, maximum Sf decreases are modeled for spring, leading to rainfall increases; on the
511 other hand, warming depletes the snowpack in the warmest and snow driest sectors of the range. Consequently,
512 data suggest a general ROS fr decrease for the majority of the SE massifs, where the snowpack is near the
513 isothermal conditions in the baseline climate period. Yet, during spring, the highest ROS fr increases are
514 detected in SW and NW, since these sectors are less exposed to radiative and turbulent heat fluxes and record
515 higher-than-average seasonal snow accumulations.

516 ROS rain generally increases due to warming, independently of the sector and elevation, being limited by the
517 number of ROS days. The largest and constant increments are observed in spring, when ROS rain increases at
518 a rate of 7, 6 and 3 % per $^{\circ}\text{C}$ for low, mid and high, respectively. ROS rain increases are explained by Sf
519 reductions, which decrease at a rate of 29 %, 22 %, and 12 % per $^{\circ}\text{C}$ for low, mid, and high elevations,
520 respectively. ROS rain maximum values are detected in SE (28 mm/day), especially in mid elevation during
521 autumn (45 mm/day), since this sector is exposed to subtropical Mediterranean flows.

522 Finally, ROS ablation shows contrasting patterns depending on the season, sector and elevation. Generally,
523 ROS ablation increases in cold snowpacks, such as those modeled in high elevation and during cold seasons
524 (autumn and winter). Here, ROS ablation follows a constant ablation rate of around $+ 10\%$ per $^{\circ}\text{C}$, due to
525 higher-than-average positive sensible and LWin heat fluxes. However, in SE and low elevations, where
526 marginal and isothermal snowpacks are found, no changes or decreases in ROS ablation are detected due to
527 snowpack magnitude reductions in a warmer climate. Results demonstrate the high snow sensitivity to climate
528 within a mid-latitude mountain range, and suggest significant changes with regards to water resources
529 management. Relevant implications in the ecosystem and socio-economic activities associated with snow
530 cover are anticipated.

531

532

533



534 **Data availability**

535 FSM2 is an open access snow model (Essery, 2015) provided at <https://github.com/RichardEssery/FSM2> (last
536 access 15 January 2023). SAFRAN climate dataset (Vernay et al., 2022) is available by AERIS at
537 <https://www.aeris-data.fr/landing-page/?uuid=865730e8-edeb-4c6b-ac58-80f95166509b#v2020.2> (last access
538 16 December 2022). Data of this work is available upon request by the first author (josepbonsoms5@ub.edu).

539 **Author contribution**

540 J.B., J.I.L.M., and E.A.G. designed the work. J.B. analyzed the data and wrote the manuscript. J.B., J.I.L.M.,
541 E.A.G., C.D.B., and M.O. provided feedback and edited the manuscript. J.I.L.M., M.O. supervised the project
542 and acquired funding.

543 **Competing interests**

544 The authors declare that they have no conflict of interest.

545 **Acknowledgements**

546 This work frames within the research topics examined by the research group “Antarctic, Artic, Alpine
547 Environments-ANTALP” (2017-SGR-1102) funded by the Government of Catalonia, HIDROIBERNIEVE
548 (CGL2017-82216-R) and MARGISNOW (PID2021-124220OB-100), from the Spanish Ministry of Science,
549 Innovation and Universities. JB is supported by a pre-doctoral University Professor FPI grant (PRE2021-
550 097046) funded by the Spanish Ministry of Science, Innovation and Universities.

551

552 **References**

553

554 Alonso-González, E., Aalstad, K., Baba, M. W., Revuelto, J., López-Moreno, J. I., Fiddes, J., et al. MuSA: The
555 Multiscale Snow Data Assimilation System (v1.0). Geoscientific Model Development Discussions, 1–43.
556 <https://doi.org/10.5194/gmd-2022-137>, 2022.

557

558 Alonso-González, E., López-Moreno, J.I., Navarro-Serrano, F., Sanmiguel-Valladolid, A., Aznárez-Balta, M.,
559 Revuelto, J., and Ceballos, A.: Snowpack Sensitivity to Temperature, Precipitation, and Solar Radiation
560 Variability over an Elevational Gradient in the Iberian Mountains, Atmos. Res., 243, 104973 <https://doi.org/10.1016/j.atmosres.2020.104973>, 2020a.

562

563 Alonso-González, E., López-Moreno, J.I., Navarro-Serrano, F., Sanmiguel-Valladolid, A., Revuelto, J.,
564 Domínguez-Castro, F., and Ceballos, A.: Snow climatology for the mountains in the Iberian Peninsula using
565 satellite imagery and simulations with dynamically downscaled reanalysis data, International Journal of
566 Climatology, 40(1), 477–491, <https://doi.org/10.1002/joc.6223>, 2019.

567

568 Alonso-González, E., López-Moreno, J. I., Navarro-Serrano, F. M., and Revuelto, J.: Impact of North Atlantic
569 Oscillation on the snowpack in Iberian Peninsula mountains, Water (Switzerland), 12,
570 <https://doi.org/10.3390/w12010105>, 2020b.



- 571 Amblar-Francés, M. P., Ramos-Calzado, P., Sanchis-Lladó, J., Hernanz-Lázaro, A., Peral-García, M. C.,
572 Navascués, B., Dominguez-Alonso, M., Pastor-Saavedra, M. A., and Rodríguez-Camino, E.: High resolution
573 climate change projections for the Pyrenees region, in: *Advances in Science and Research*, 191–208,
574 <https://doi.org/10.5194/asr-17-191-2020>, 2020.
- 575
- 576 Barnett, T.P., Adam, J.C., and Lettenmaier, D.P., Potential impacts of a warming climate on water availability
577 in snow-dominated regions. *Nature*. <https://doi.org/10.1038/nature04141>, 2005.
- 578 Bartsch, A., Kumpula, T., Forbes, B. C., and Stammler, F.: Detection of snow surface thawing and refreezing
579 in the Eurasian arctic with QuikSCAT: Implications for reindeer herding. *Ecological Applications*, 20, 2346–
580 2358, <https://doi.org/10.1890/09-1927.1>, 2010.
- 581 Beniston, M. and Stoffel, M.: Rain-on-snow events, floods and climate change in the Alps: Events may increase
582 with warming up to 4 °C and decrease thereafter, *Science of the Total Environment*, 571, 228–236,
583 <https://doi.org/10.1016/j.scitotenv.2016.07.146>, 2016.
- 584 Beniston, M., Farinotti, D., Stoffel, M., Andreassen, L. M., Coppola, E., Eckert, N., Fantini, A., Giacona, F.,
585 Hauck, C., Huss, M., Huwald, H., Lehning, M., López-Moreno, J. I., Magnusson, J., Marty, C., Morán-Tejeda,
586 E., Morin, S., Naaim, M., Provenzale, A., Rabatel, A., Six, D., Stötter, J., Strasser, U., Terzago, S., and Vincent,
587 C.: The European mountain cryosphere: A review of its current state, trends, and future challenges,
588 <https://doi.org/10.5194/tc-12-759-2018>, 2018.
- 589 Bieniek, P. A., Bhatt, U. S., Walsh, J. E., Lader, R., Griffith, B., Roach, J. K., and Thoman, R. L.: Assessment
590 of Alaska rain-on-snow events using dynamical downscaling, *J Appl Meteorol Climatol*, 57, 1847–1863,
591 <https://doi.org/10.1175/JAMC-D-17-0276.1>, 2018.
- 592 Bintanja, R. and Andry, O.: Towards a rain-dominated Arctic, *Nat Clim Chang*, 7, 263–267,
593 <https://doi.org/10.1038/nclimate3240>, 2017.
- 594 Bonsoms, J., Franch, F. S., and Oliva, M.: Snowfall and snow cover evolution in the eastern pre-pyrenees (Ne
595 iberian peninsula), *Geographical Research Letters*, 47, 291–307, <https://doi.org/10.18172/cig.4879>, 2021a.
- 596 Bonsoms, J., González, S., Prohom, M., Esteban, P., Salvador-Franch, F., López-Moreno, J. I., and Oliva, M.:
597 Spatio-temporal patterns of snow in the Catalan Pyrenees (NE Iberia), *International Journal of Climatology*,
598 41, 5676–5697, <https://doi.org/10.1002/joc.7147>, 2021b.
- 599 Bonsoms, J., López-Moreno, J. I., González, S., and Oliva, M.: Increase of the energy available for snow
600 ablation in the Pyrenees (1959–2020) and its relation to atmospheric circulation, *Atmos Res*, 275,
601 <https://doi.org/10.1016/j.atmosres.2022.106228>, 2022a.
- 602 Bonsoms, J., López-Moreno, J., and Alonso-González, E.: Snowpack sensitivity to climate change during
603 compound cold-hot and wet-dry seasons, *EGUsphere (preprint)*, <https://doi.org/10.5194/egusphere-2022-851>,
604 2022b.
- 605 Buisan, S.T., López-Moreno, J.I., Sanz, M.A. and Korchendorfer, J. Impact of weather type variability on
606 winter precipitation, temperature and annual snowpack in the Spanish Pyrenees. *Climate Research*, 69, 79–92.
607 <https://doi.org/10.3354/cr01391>, 2016.
- 608 Bjerke JW, Treharne R, Vikhamar-Schuler D, Karlsen S R, Ravolainen V, Bokhorst S, Phoenix G K, Bochenek
609 Z and Tømmervik H 2017 Understanding the drivers of extensive plant damage in boreal and Arctic
610 ecosystems: insights from field surveys in the aftermath of damage *Sci. Total Environ.* 599 1965–76.



- 611 Ceron, J. P., Tanguy, G., Franchistéguy, L., Martin, E., Regimbeau, F., and Vidal, J. P.: Hydrological seasonal
612 forecast over France: Feasibility and prospects, *Atmospheric Science Letters*, 11, 78–82,
613 <https://doi.org/10.1002/asl.256>, 2010.
- 614 Cohen, J., Ye, H., and Jones, J.: Trends and variability in rain-on-snow events, *Geophys Res Lett*, 42, 7115–
615 7122, <https://doi.org/10.1002/2015GL065320>, 2015.
- 616 Collados-Lara, A. J., Pulido-Velazquez, D., Pardo-Igúzquiza, E., and Alonso-González, E.: Estimation of the
617 spatio-temporal dynamic of snow water equivalent at mountain range scale under data scarcity, *Science of the*
618 *Total Environment*, 741, <https://doi.org/10.1016/j.scitotenv.2020.140485>, 2020.
- 619 Conway, H. and Raymond, C. F.: Snow stability during rain, *Journal of Glaciology*, 39, 635–642,
620 <https://doi.org/10.3189/s0022143000016531>, 1993.
- 621 Corripio, J. G. and López-Moreno, J. I.: Analysis and predictability of the hydrological response of mountain
622 catchments to heavy rain on snow events: A case study in the Spanish Pyrenees, *Hydrology*, 4,
623 <https://doi.org/10.3390/hydrology4020020>, 2017.
- 624 Crawford, A. D., Alley, K. E., Cooke, A. M., and Serreze, M. C.: Synoptic Climatology of Rain-on-Snow
625 Events in Alaska, <https://doi.org/10.1175/MWR-D-19, 2020>.
- 626 Deschamps-Berger, C., Cluzet, B., Dumont, M., Lafaysse, M., Berthier, E., Fanise, P., and Gascoin, S.:
627 Improving the Spatial Distribution of Snow Cover Simulations by Assimilation of Satellite Stereoscopic
628 Imagery, *Water Resour. Res.*, 58, e2021WR030271, <https://doi.org/10.1029/2021WR030271>, 2022.
629
- 630 Del Barrio, G., Creus, J., and Puigdefabregas, J.: Thermal Seasonality of the High Mountain Belts of the
631 Pyrenees, *Mt. Res. Dev.*, 10, 227–233, 1990.
- 632 Devers, A., Vidal, J. P., Lauvernet, C., and Vannier, O.: FYRE Climate: A high-resolution reanalysis of daily
633 precipitation and temperature in France from 1871 to 2012, *Climate of the Past*, 17, 1857–1879,
634 <https://doi.org/10.5194/cp-17-1857-2021>, 2021.
- 635 Durand, Y., Giraud, G., Brun, E., Mérindol, L., and Martin, E.: A computer-based system simulating snowpack
636 structures as a tool for regional avalanche forecasting, *Journal of Glaciology*, 45, 469–484,
637 <https://doi.org/10.3189/s0022143000001337>, 1999.
- 638 Durand, Y., Laternser, M., Giraud, G., Etchevers, P., Lesaffre, B., and Mérindol, L.: Reanalysis of 44 yr of
639 climate in the French Alps (1958-2002): Methodology, model validation, climatology, and trends for air
640 temperature and precipitation, *J Appl Meteorol Climatol*, 48, 429–449,
641 <https://doi.org/10.1175/2008JAMC1808.1>, 2009.
- 642 Essery, R.: A factorial snowpack model (FSM 1.0), *Geosci Model Dev*, 8, 3867–3876,
643 <https://doi.org/10.5194/gmd-8-3867-2015>, 2015.
644
- 645 Essery, R., Kim, H., Wang, L., Bartlett, P., Boone, A., Brutel-Vuilmet, C., Burke, E., Cuntz, M., Decharme,
646 B., Dutra, E., Fang, X., Gusev, Y., Hagemann, S., Haverd, V., Kontu, A., Krinner, G., Lafaysse, M., Lejeune,
647 Y., Marke, T., Marks, D., Marty, C., Menard, C. B., Nasonova, O., Nitta, T., Pomeroy, J., Schädler, G.,
648 Semenov, V., Smirnova, T., Swenson, S., Turkov, D., Wever, N., and Yuan, H.: Snow cover duration trends
649 observed at sites and predicted by multiple models, *Cryosphere*, 14, 4687–4698, [https://doi.org/10.5194/tc-](https://doi.org/10.5194/tc-14-4687-2020)
650 [14-4687-2020](https://doi.org/10.5194/tc-14-4687-2020), 2020.
- 651 Freudiger, D., Kohn, I., Stahl, K., and Weiler, M.: Large-scale analysis of changing frequencies of rain-on-



- 652 snow events with flood-generation potential, *Hydrol Earth Syst Sci*, 18, 2695–2709,
653 <https://doi.org/10.5194/hess-18-2695-2014>, 2014.
- 654 García-Ruiz, J. M., López-Moreno, J. I., Vicente-Serrano, S. M., Lasanta-Martínez, T. and Beguería, S.
655 Mediterranean water resources in a global change scenario, *Earth Sci. Rev.*, 105(3–4), 121–139,
656 <https://doi.org/10.1016/j.earscirev.2011.01.006>, 2011.
- 657 Garvelmann, J., Pohl, S., and Weiler, M.: Variability of observed energy fluxes during rain-on-snow and clear
658 sky snowmelt in a midlatitude mountain environment, *J Hydrometeorol*, 15, 1220–1237,
659 <https://doi.org/10.1175/JHM-D-13-0187.1>, 2014.
- 660 Günther, D., Marke, T., Essery, R., and Strasser, U.: Uncertainties in Snowpack Simulations—Assessing the
661 Impact of Model Structure, Parameter Choice, and Forcing Data Error on Point-Scale Energy Balance Snow
662 Model Performance, *Water Resour Res*, 55, 2779–2800, <https://doi.org/10.1029/2018WR023403>, 2019.
- 663 Habets, F., Boone, A., Champeaux, J. L., Etchevers, P., Franchistéguy, L., Leblois, E., Ledoux, E., le Moigne,
664 P., Martin, E., Morel, S., Noilhan, J., Seguí, P. Q., Rousset-Regimbeau, F., and Viennot, P.: The SAFRAN-
665 ISBA-MODCOU hydrometeorological model applied over France, *Journal of Geophysical Research*
666 *Atmospheres*, 113, <https://doi.org/10.1029/2007JD008548>, 2008.
- 667 Hansen, B.B., Grøtan, V., Aanes, R., et al., 2013. Climate events synchronize the dynamics of a resident
668 vertebrate community in the High Arctic. *Science* 339, 313–315.
- 669 Hansen, B.B., Isaksen, K., Benestad, R.E., et al., 2014. Warmer and wetter winters: characteristics and
670 implications of an extreme weather event in the High Arctic. *Environ. Res. Lett.* 9, 114021.
- 671 Immerzeel, W. W., Lutz, A. F., Andrade, M., Bahl, A., Biemans, H., Bolch, T., Hyde, S., Brumby, S., Davies,
672 B. J., Elmore, A. C., Emmer, A., Feng, M., Fernández, A., Haritashya, U., Kargel, J. S., Koppes, M.,
673 Kraaijenbrink, P. D. A., Kulkarni, A. v., Mayewski, P. A., Nepal, S., Pacheco, P., Painter, T. H., Pellicciotti, F.,
674 Rajaram, H., Rupper, S., Sinisalo, A., Shrestha, A. B., Viviroli, D., Wada, Y., Xiao, C., Yao, T., and Baillie, J.
675 E. M.: Importance and vulnerability of the world’s water towers, *Nature*, 577, 364–369,
676 <https://doi.org/10.1038/s41586-019-1822-y>, 2020.
- 677 IPCC: High Mountain Areas, in: *The Ocean and Cryosphere in a Changing Climate*, Cambridge University
678 Press, 131–202, <https://doi.org/10.1017/9781009157964.004>, 2022.
- 679 Jennings, K. S., Winchell, T. S., Livneh, B., and Molotch, N. P.: Spatial variation of the rain-snow temperature
680 threshold across the Northern Hemisphere, *Nat Commun*, 9, <https://doi.org/10.1038/s41467-018-03629-7>,
681 2018.
- 682 il Jeong, D. and Sushama, L.: Rain-on-snow events over North America based on two Canadian regional
683 climate models, *Clim Dyn*, 50, 303–316, <https://doi.org/10.1007/s00382-017-3609-x>, 2018.
- 684 Kohler, J. and Aanes, R.: Effect of winter snow and ground-icing on a Svalbard reindeer population: Results
685 of a simple snowpack model, in: *Arctic, Antarctic, and Alpine Research*, 333–341,
686 [https://doi.org/10.1657/1523-0430\(2004\)036\[0333:EOWSAG\]2.0.CO;2](https://doi.org/10.1657/1523-0430(2004)036[0333:EOWSAG]2.0.CO;2), 2004.
- 687 Lemus-Canovas, M., Lopez-Bustins, J. A., Trapero, L., and Martín-Vide, J.: Combining circulation weather
688 types and daily precipitation modelling to derive climatic precipitation regions in the Pyrenees, *Atmos Res*,
689 220, 181–193, <https://doi.org/10.1016/j.atmosres.2019.01.018>, 2019.
- 690 Lemus-Canovas, M., Lopez-Bustins, J. A., Martín-Vide, J., Halifa-Marin, A., Insua-Costa, D., Martínez-



- 691 Artigas, J., Trapero, L., Serrano-Notivol, R., and Cuadrat, J. M.: Characterisation of extreme precipitation
692 events in the Pyrenees: From the local to the synoptic scale, *Atmosphere (Basel)*, 12,
693 <https://doi.org/10.3390/atmos12060665>, 2021.
- 694 Li, D., Lettenmaier, D. P., Margulis, S. A., and Andreadis, K.: The Role of Rain-on-Snow in Flooding Over
695 the Conterminous United States, *Water Resour Res*, 55, 8492–8513, <https://doi.org/10.1029/2019WR024950>,
696 2019.
- 697 Llasat, M. C., Marcos, R., Llasat-Botija, M., Gilbert, J., Turco, M., and Quintana-Seguí, P.: Flash flood
698 evolution in North-Western Mediterranean, *Atmos Res*, 149, 230–243,
699 <https://doi.org/10.1016/j.atmosres.2014.05.024>, 2014.
- 700 López-Moreno, J. I.: Recent variations of snowpack depth in the central Spanish Pyrenees, *Arct Antarct Alp*
701 *Res*, 37, 253–260, [https://doi.org/10.1657/1523-0430\(2005\)037\[0253:RVOSDI\]2.0.CO;2](https://doi.org/10.1657/1523-0430(2005)037[0253:RVOSDI]2.0.CO;2), 2005.
- 702 López-Moreno, J. I., Pomeroy, J. W., Revuelto, J., and Vicente-Serrano, S. M.: Response of snow processes to
703 climate change: Spatial variability in a small basin in the Spanish Pyrenees, *Hydrol Process*, 27, 2637–2650,
704 <https://doi.org/10.1002/hyp.9408>, 2013.
- 705 López-Moreno, J. I., Pomeroy, J. W., Morán-Tejeda, E., Revuelto, J., Navarro-Serrano, F. M., Vidaller, I., and
706 Alonso-González, E.: Changes in the frequency of global high mountain rain-on-snow events due to climate
707 warming, *Environmental Research Letters*, 16, <https://doi.org/10.1088/1748-9326/ac0dde>, 2021.
- 708 López-Moreno, J.I., Soubeyroux, J.M., Gascoïn, S., Alonso-González, E., Durán-Gómez, N., Lafaysse, M.,
709 Vernay, M., Carmagnola, C. and Morin, S. Long-term trends (1958–2017) in snow cover duration and depth
710 in the Pyrenees. *International Journal of Climatology*, 40, 1–15. <https://doi.org/10.1002/joc.6571>, 2020.
- 711 López-Moreno, J.I., and Vicente-Serrano, S.M.: Atmospheric circulation influence on the interannual
712 variability of snowpack in the Spanish Pyrenees during the second half of the twentieth century, *Nord. Hydrol.*,
713 38 (1), 38–44, <https://doi.org/10.2166/nh.2007.030>, 2007.
- 714 López-Moreno, J.I., and Latron, J., 2008. Spatial heterogeneity in snow water equivalent induced by forest
715 canopy in a mixed beech-fir stand in the Pyrenees. *Ann. Glaciol.* 49 (1), 83–90,
716 <https://doi.org/10.3189/172756408787814951>, 2008.
- 717 Loukas, A., Vasiliades, L., and Dalezios, N. R.: Potential climate change impacts on flood producing
718 mechanisms in southern British Columbia, Canada using the CGCMA1 simulation results, *J. Hydrol.*, 259,
719 163–188, [https://doi.org/10.1016/S0022-1694\(01\)00580-7](https://doi.org/10.1016/S0022-1694(01)00580-7), 2002
- 720 Lundquist, J. D., Dickerson-Lange, S. E., Lutz, J. A., and Cristea, N. C.: Lower forest density enhances snow
721 retention in regions with warmer winters: A global framework developed from plot-scale observations and
722 modeling, *Water Resour Res*, 49, 6356–6370, <https://doi.org/10.1002/wrcr.20504>, 2013.
- 723 Lynn, E., Cuthbertson, A., He, M., Vasquez, J. P., Anderson, M. L., Coombe, P., Abatzoglou, J. T., and Hatchett,
724 B. J.: Technical note: Precipitation-phase partitioning at landscape scales to regional scales, *Hydrol Earth Syst*
725 *Sci*, 24, 5317–5328, <https://doi.org/10.5194/hess-24-5317-2020>, 2020.
- 726 Matiu, M., Crespi, A., Bertoldi, G., Carmagnola, C.M., Marty, C., Morin, S., Schöner, W., Cat Berro, D.,
727 Chiogna, G., De Gregorio, L., Kotlarski, S., Majone, B., Resch, G., Terzago, S., Valt, M., Beozzo, W.,
728 Cianfarra, P., Gouttevin, I., Marcolini, G., Notarnicola, C., Petitta, M., Scherrer, S.C., Strasser, U., Winkler,
729 M., Zebisch, M., Cicogna, A., Cremonini, R., Debernardi, A., Faletto, M., Gaddo, M., Giovannini, L., Mercalli,



- 730 L., Soubeyroux, J.-M., Susnik, A., Trenti, A., Urbani, S., Weigluni, V. Observed snow depth trends in the
731 European Alps 1971 to 2019. *Cryosphere*, 1–50. <https://doi.org/10.5194/tc-2020-289>, 2020.
- 732 Marks, D., Link, T., Winstral, A., and Garen, D.: Simulating snowmelt processes during rain-on-snow over a
733 semi-arid mountain basin, 1992.
- 734 Marty, C., Schlögl, S., Bavay, M., and Lehning, M.: How much can we save? Impact of different emission
735 scenarios on future snow cover in the Alps, *Cryosphere*, 11, 517–529, <https://doi.org/10.5194/tc-11-517-2017>,
736 2017.
- 737 Mazurkiewicz, A. B., Callery, D. G., and McDonnell, J. J.: Assessing the controls of the snow energy balance
738 and water available for runoff in a rain-on-snow environment, *J Hydrol (Amst)*, 354, 1–14,
739 <https://doi.org/10.1016/j.jhydrol.2007.12.027>, 2008.
- 740 Mazzotti, G., Essery, R., Webster, C., Malle, J., and Jonas, T.: Process-Level Evaluation of a Hyper-Resolution
741 Forest Snow Model Using Distributed Multisensor Observations, *Water Resour Res*, 56,
742 <https://doi.org/10.1029/2020WR027572>, 2020.
- 743 McCabe, G. J., Clark, M. P., and Hay, L. E.: Rain-on-snow events in the Western United-States,
744 <https://doi.org/10.1175/BAMS-88-3-319>, 2007.
- 745 Mooney, P. A. and Li, L.: Near future changes to rain-on-snow events in Norway, *Environmental Research*
746 *Letters*, 16, <https://doi.org/10.1088/1748-9326/abfdeb>, 2021.
- 747 Morán-Tejeda, E., López-Moreno, J. I., Stoffel, M., and Beniston, M.: Rain-on-snow events in Switzerland:
748 Recent observations and projections for the 21st century, *Clim Res*, 71, 111–125,
749 <https://doi.org/10.3354/cr01435>, 2016.
- 750 Morán-Tejeda, E., Fassnacht, S. R., Lorenzo-Lacruz, J., López-Moreno, J. I., García, C., Alonso-González, E.,
751 and Collados-Lara, A. J.: Hydro-meteorological characterization of major floods in Spanish mountain rivers,
752 *Water (Switzerland)*, 11, <https://doi.org/10.3390/W11122641>, 2019.
- 753 Morin, S., Horton, S., Techel, F., Bavay, M., Coléou, C., Fierz, C., Gobiet, A., Hagenmuller, P., Lafaysse, M.,
754 Ližar, M., Mitterer, C., Monti, F., Müller, K., Olefs, M., Snook, J. S., van Herwijnen, A., and Vionnet, V.:
755 Application of physical snowpack models in support of operational avalanche hazard forecasting: A status
756 report on current implementations and prospects for the future,
757 <https://doi.org/10.1016/j.coldregions.2019.102910>, 2020.
- 758 Musselman, K. N., Clark, M. P., Liu, C., Ikeda, K., and Rasmussen, R.: Slower snowmelt in a warmer world,
759 *Nat Clim Chang*, 7, 214–219, <https://doi.org/10.1038/nclimate3225>, 2017a.
- 760 Musselman, K. N., Keitholotch, N. P., Mar, N., and Mgulis, S. A.: Snowmelt response to simulated warming
761 across a large elevation gradient, southern sierra Nevada, California, *Cryosphere*, 11, 2847–2866,
762 <https://doi.org/10.5194/tc-11-2847-2017>, 2017b.
- 763 Musselman, K. N., Lehner, F., Ikeda, K., Clark, M. P., Prein, A. F., Liu, C., Barlage, M., and Rasmussen, R.:
764 Projected increases and shifts in rain-on-snow flood risk over western North America,
765 <https://doi.org/10.1038/s41558-018-0236-4>, 2018.
- 766 Navarro-Serrano, F. and López-Moreno, J. I.: Análisis espacio-temporal de los eventos de nevadas en el pirineo
767 Español y su relación con la circulación atmosférica, *Cuadernos de Investigacion Geografica*, 43, 233–254,
768 <https://doi.org/10.18172/cig.3042>, 2017.



- 769 Ohba, M. and Kawase, H.: Rain-on-Snow events in Japan as projected by a large ensemble of regional climate
770 simulations, *Clim Dyn*, 55, 2785–2800, <https://doi.org/10.1007/s00382-020-05419-8>, 2020.
- 771
- 772 OPCC-CTP. Climate change in the Pyrenees: Impacts, vulnerabilities and adaptation bases of knowledge for
773 the future climate change adaptation strategy in the Pyrenees. 2018. 147. Jaca, Spain.
774 <https://www.opccctp.org/sites/default/files/editor/opcc-informe-en-paginas.pdf>. (last acces December 25,
775 2022)
- 776 Pall, P., Tallaksen, L. M., and Stordal, F.: A Climatology of Rain-on-Snow Events for Norway,
777 <https://doi.org/10.1175/JCLI-D-18, 2019>.
- 778 Pepin, N. C., Arnone, E., Gobiet, A., Haslinger, K., Kotlarski, S., Notarnicola, C., Palazzi, E., Seibert, P.,
779 Serafin, S., Schöner, W., Terzago, S., Thornton, J. M., Vuille, M., and Adler, C.: Climate Changes and Their
780 Elevational Patterns in the Mountains of the World, <https://doi.org/10.1029/2020RG000730>, 2022.
- 781 Peña-Angulo, D., Vicente-Serrano, S., Domínguez-Castro, F., Murphy, C., Reig, F., Trambly, Y., Trigo, R.,
782 Luna, M.Y., Turco, M., Noguera, I., Aznárez-Balta, M., Garcia-Herrera, R., Tomas-Burguera, M. and
783 Kenawy, A. Long-term precipitation in Southwestern Europe reveals no clear trend attributable to
784 anthropogenic forcing. *Environmental Research Letters*, 15, 094070 <https://doi.org/10.1088/1748-9326/ab9c4f>,
785 2020.
- 786 Pomeroy, J. W., Fang, X., and Rasouli, K.: Sensitivity of snow processes to warming in the Canadian Rockies,
787 2015.
- 788 Pomeroy, J. W., Fang, X., and Marks, D. G.: The cold rain-on-snow event of June 2013 in the Canadian Rockies
789 — characteristics and diagnosis, *Hydrol Process*, 30, 2899–2914, <https://doi.org/10.1002/hyp.10905>, 2016.
- 790 Quintana-Seguí, P., le Moigne, P., Durand, Y., Martin, E., Habets, F., Baillon, M., Canellas, C., Franchisteguy,
791 L., and Morel, S.: Analysis of near-surface atmospheric variables: Validation of the SAFRAN analysis over
792 France, *J Appl Meteorol Climatol*, 47, 92–107, <https://doi.org/10.1175/2007JAMC1636.1>, 2008.
- 793 Quintana-Seguí, P., Turco, M., Herrera, S., and Miguez-Macho, G.: Validation of a new SAFRAN-based
794 gridded precipitation product for Spain and comparisons to Spain02 and ERA-Interim, *Hydrol Earth Syst Sci*,
795 21, 2187–2201, <https://doi.org/10.5194/hess-21-2187-2017>, 2017.
- 796 Rasouli, K., Pomeroy, J. W., and Whitfield, P. H.: Hydrological responses of headwater basins to monthly
797 perturbed climate in the North American Cordillera, *J Hydrometeorol*, 20, 863–882,
798 <https://doi.org/10.1175/JHM-D-18-0166.1>, 2019.
- 799 Rennert, K. J., Roe, G., Putkonen, J., and Bitz, C. M.: Soil thermal and ecological impacts of rain on snow
800 events in the circumpolar arctic, *J Clim*, 22, 2302–2315, <https://doi.org/10.1175/2008JCLI2117.1>, 2009.
- 801 Réveillet, M., Dumont, M., Gascoin, S., Lafaysse, M., Nabat, P., Ribes, A., Nheili, R., Tuzet, F., Ménégoz, M.,
802 Morin, S., Picard, G., and Ginoux, P.: Black carbon and dust alter the response of mountain snow cover under
803 climate change, *Nat Commun*, 13, <https://doi.org/10.1038/s41467-022-32501-y>, 2022.
- 804 Revuelto, J., Lecourt, G., Lafaysse, M., Zin, I., Charrois, L., Vionnet, V., Dumont, M., Rabatel, A., Six, D.,
805 Condom, T., Morin, S., Viani, A., and Sirguey, P.: Multi-criteria evaluation of snowpack simulations in
806 complex alpine terrain using satellite and in situ observations, *Remote Sens (Basel)*, 10,
807 <https://doi.org/10.3390/rs10081171>, 2018.



- 808 Roe, G. H. and Baker, M. B.: Microphysical and Geometrical Controls on the Pattern of Orographic
809 Precipitation, 2006.
- 810 Sanmiguel-Valladolid, A., McPhee, J., Esmeralda Ojeda Carreño, P., Morán-Tejeda, E., Julio Camarero, J., and
811 López-Moreno, J. I.: Sensitivity of forest–snow interactions to climate forcing: Local variability in a Pyrenean
812 valley, *J Hydrol (Amst)*, 605, <https://doi.org/10.1016/j.jhydrol.2021.127311>, 2022.
- 813 Schirmer, M., Winstral, A., Jonas, T., Burlando, P., and Peleg, N.: Natural climate variability is an important
814 aspect of future projections of snow water resources and rain-on-snow events, *Cryosphere*, 16, 3469–3488,
815 <https://doi.org/10.5194/tc-16-3469-2022>, 2022.
- 816 Schöner, W., Koch, R., Matulla, C., Marty, C., and Tilg, A. M.: Spatio-temporal patterns of snow depth within
817 the Swiss-Austrian Alps for the past half century (1961 to 2012) and linkages to climate change, *International*
818 *Journal of Climatology*, 39, 1589–1603, <https://doi.org/10.1002/joc.5902>, 2019.
- 819 Serrano-Notivoli, R., Buisan, S.T., Abad-Pérez, L.M., Sierra-Álvarez, E., Rodríguez-Ballesteros, C., López-
820 Moreno, J.I. and Cuadrat, J.M. Tendencias recientes en precipitación, temperatura y nieve de alta montaña en
821 los Pirineos (Refugio de Góriz, Huesca). In: *El clima: aire, agua, tierra y fuego*. Madrid, Spain: Asociación
822 Española de Climatología y Ministerio para la Transición Ecológica – Agencia Estatal de Meteorología, pp.
823 267, 1060–280, 2018.
- 824 Serrano-Notivoli, R., Mora, D., Ollero, A., Sánchez-Fabre, M., Sanz, P., and Saz, M.: Floodplain occupation
825 and flooding in the central Pyrenees, *Cuadernos de Investigacion Geografica*, 43, 309–328,
826 <https://doi.org/10.18172/cig.3057>, 2017.
- 827 Serreze, M. C., Gustafson, J., Barrett, A. P., Druckenmiller, M. L., Fox, S., Voveris, J., Stroeve, J., Sheffield,
828 B., Forbes, B. C., Rasmus, S., Laptander, R., Brook, M., Brubaker, M., Temte, J., McCrystall, M. R., and
829 Bartsch, A.: Arctic rain on snow events: Bridging observations to understand environmental and livelihood
830 impacts, *Environmental Research Letters*, 16, <https://doi.org/10.1088/1748-9326/ac269b>, 2021.
- 831 Shanley, J. B. and Chalmers, A.: The effect of frozen soil on snowmelt runoff at Sleepers River, Vermont 1999.
- 832 Singh, P., Spitzbart, G., Hübl, H., and Weinmeister, H. W.: Hydrological response of snowpack under rain-on-
833 snow events: a field study, *Journal of Hydrology*, 1–20 pp., 1997.
- 834 Smyth, E. J., Raleigh, M. S., and Small, E. E. (2020). Improving SWE estimation with data assimilation: The
835 influence of snow depth observation timing and uncertainty. *Water Resources Research*, 56, e2019WR026853.
836 <https://doi.org/10.1029/2019WR026853>
- 837 Spandre, P., François, H., Verfaillie, D., Lafaysse, M., Déqué, M., Eckert, N., George, E., and Morin, S.:
838 Climate controls on snow reliability in French Alps ski resorts, *Sci Rep*, 9, <https://doi.org/10.1038/s41598-019-44068-8>, 2019.
- 840 Stewart, I. T.: Changes in snowpack and snowmelt runoff for key mountain regions,
841 <https://doi.org/10.1002/hyp.7128>, 2009.
- 842 Surfleet, C. G. and Tullos, D.: Variability in effect of climate change on rain-on-snow peak flow events in a
843 temperate climate, *J Hydrol (Amst)*, 479, 24–34, <https://doi.org/10.1016/j.jhydrol.2012.11.021>, 2013.
- 844 Szczypta, C., Gascoïn, S., Houet, T., Hagolle, O., Dejoux, J.-F., Vigneau, C., and Fanise, P.: Impact of climate
845 and land cover changes on snow cover in a small Pyrenean catchment, *J. Hydrol.*, 521, 84–99,
846 [doi:10.1016/j.jhydrol.2014.11.060](https://doi.org/10.1016/j.jhydrol.2014.11.060), 2015.



847 Verfaillie, D., Lafaysse, M., Déqué, M., Eckert, N., Lejeune, Y., and Morin, S.: Multi-component ensembles
848 of future meteorological and natural snow conditions for 1500 m altitude in the Chartreuse mountain range,
849 Northern French Alps, *Cryosphere*, 12, 1249–1271, <https://doi.org/10.5194/tc-12-1249-2018>, 2018.

850 Vernay, M., Lafaysse, M., Monteiro, D., Hagenmuller, P., Nheili, R., Samacoïts, R., Verfaillie, D., and Morin,
851 S.: The S2M meteorological and snow cover reanalysis over the French mountainous areas: description and
852 evaluation (1958-2021), *Earth Syst Sci Data*, 14, 1707–1733, <https://doi.org/10.5194/essd-14-1707-2022>,
853 2022.

854 Vicente-Serrano, S.M., Rodríguez-Camino, E., Domínguez-Castro, F., El Kenawy, A., Azorín-Molina, C. An
855 updated review on recent trends in observational surface atmospheric variables and their extremes over Spain.
856 *Cuadernos de Investigación Geográfica (Geographical Research Letters)* 43 (1), 209-232.
857 <https://doi.org/10.18172/cig.3134>, 2017.

858 Vidaller, I., Revuelto, J., Izagirre, E., Rojas-Heredia, F., Alonso-González, E., Gascoïn, S., René, P., Berthier,
859 E., Rico, I., Moreno, A., Serrano, E., Serreta, A., López-Moreno, J.I. Toward an ice-free mountain range:
860 Demise of Pyrenean glaciers during 2011–2020. *J. Geophys. Res. Lett.* 48, e2021GL094339
861 <https://doi.org/10.1029/2021GL094339>, 2021.

862 Viviroli, D., Archer, D. R., Buytaert, W., Fowler, H. J., Greenwood, G. B., Hamlet, A. F., Huang, Y.,
863 Koboltschnig, G., Litaor, M. I., López-Moreno, J. I., Lorentz, S., Schädler, B., Schreier, H., Schwaiger, K.,
864 Vuille, M., and Woods, R.: Climate change and mountain water resources: Overview and recommendations
865 for research, management and policy, *Hydrol Earth Syst Sci*, 15, 471–504, [https://doi.org/10.5194/hess-15-](https://doi.org/10.5194/hess-15-471-2011)
866 471-2011, 2011.

867 Westermann, S., Boike, J., Langer, M., Schuler, T. v., and Eitzelmüller, B.: Modeling the impact of wintertime
868 rain events on the thermal regime of permafrost, *Cryosphere*, 5, 945–959, [https://doi.org/10.5194/tc-5-945-](https://doi.org/10.5194/tc-5-945-2011)
869 2011, 2011.

870 Wipf, S. and Rixen, C.: A review of snow manipulation experiments in Arctic and alpine tundra ecosystems,
871 <https://doi.org/10.1111/j.1751-8369.2010.00153.x>, 2010.

872 Wu, X., Che, T., Li, X., Wang, N., and Yang, X.: Slower Snowmelt in Spring Along With Climate Warming
873 Across the Northern Hemisphere, *Geophys Res Lett*, 45, 12,331-12,339,
874 <https://doi.org/10.1029/2018GL079511>, 2018.

875 Würzer, S., Jonas, T., Wever, N., and Lehning, M.: Influence of initial snowpack properties on runoff formation
876 during rain-on-snow events, *J Hydrometeorol*, 17, 1801–1815, <https://doi.org/10.1175/JHM-D-15-0181.1>,
877 2016.

878